DOI: 10.18462/iir.gl2022.0197

Investigation of non-equilibrium effects during the depressurization of carbon dioxide

Alexandra M. LOG*[(a)], Svend T. MUNKEJORD [(b)], Morten HAMMER[(b)], Armin HAFNER [(a)], Han DENG[(b)], Anders AUSTEGARD[(b)]

[(a)] NTNU, Department of Energy and Process Engineering
Trondheim, NO-7491, Norway
[(b)] SINTEF Energy Research
Trondheim, NO-7465, Norway
*Corresponding author: alexandra.m.log@ntnu.no

ABSTRACT

Predicting the phase change of liquid CO_2 during depressurization is highly relevant for the application in refrigeration units and for safety analysis in the context of CO_2 capture and storage (CCS). For abrupt depressurization processes, nucleation of gas will not occur at equilibrium and the liquid becomes superheated. In this work, we analyze the experimental results of depressurization tests conducted in the ECCSEL depressurization facility in Trondheim for pure CO_2 and determine the degree of superheat reached in the tests. The experiments include depressurization from 11-12 MPa to atmospheric pressure at different temperatures and the thermodynamic path in one of the cases passes near the critical point. The results agree well with the nucleation rate predicted by classical nucleation theory.

Keywords: Carbon dioxide, expansion, depressurization, phase change, superheat, nucleation.

1. INTRODUCTION

Studying the phase-change behaviour of liquid CO_2 during expansion is relevant in several industrial applications. Examples include the application of CO_2 as a natural refrigerant, and for safety analysis of CO_2-carrying pipelines as part of CO_2 capture and storage (CCS) systems. In various depressurization tests of liquid CO_2, significant degrees of superheat are observed before gas forms and two-phase flow is established. The delayed nucleation leads to two-phase flow occurring at a lower pressure than assumed by equilibrium models. For safety analyses and process optimization, it is key to predict exactly when phase change occurs, as two-phase flow is much slower than single-phase flow and the inception of phase change therefore largely determines the fluid state during depressurization, and, among other things, the resulting flow rates.

In the effort to provide more data on the non-equilibrium phase-change behaviour of liquid CO_2, we study depressurization tests conducted at the ECCSEL depressurization facility, which has dense and accurate instrumentation to dynamically capture pressure and temperature (Munkejord et al., 2020). The tests are conducted with pure CO_2 and include initial conditions from 10 MPa - 12 MPa and 283 K - 313 K. We focus on pressure measurements within a very short timeframe ($\approx$ 5 ms) where gas nucleation can be observed in all the tests. Using pressure measurements to estimate when nucleation occurs contrasts with the more common method of estimating the point of nucleation based on the assumption that it coincides with critical flow. As critical flow and nucleation do not necessarily coincide (though they often do), the present method is thought to better represent the physics. To provide relevant references for the experimental results, we compare the pressure data to the prediction of the homogeneous equilibrium model, and we compare the point of nucleation to the superheat limit predicted by classical nucleation theory.

The paper is structured as follows. In Section 2 the ECCSEL depressurization facility is briefly described, in Section 3, the homogeneous equilibrium model and classical nucleation theory are outlined, in Section 4 the experimental results are presented and analyzed, and finally concluding remarks are given in Section 5.

2. EXPERIMENTAL SETUP AND INSTRUMENTATION

In this section, we briefly describe the experimental setup and instrumentation for the depressurization experiments. A more detailed description is presented by Munkejord et al. (2020).

2.1. Experimental setup and procedure

The ECCSEL depressurization facility consists of a gas supply with mass flow controllers, a compression and cooling system for achieving the desired experimental conditions, and a test section with a rupture disk at the open end. The test section is a tube made of 11 stainless steel pipes providing a total length of 61.67 m. These pipes have an inner diameter of 40.8 mm, an outer diameter of 48.3 mm, and were honed to a mean roughness of $R_a = 0.2\ \mu$m - $0.3\ \mu$m. The tube is wrapped in heating cables and insulated with a 60 mm thick layer of glass wool. In Figure 1, an overview of the setup is shown. The facility is designed for a maximum operating pressure of 20 MPa and initial temperatures within 5 °C to 40 °C.

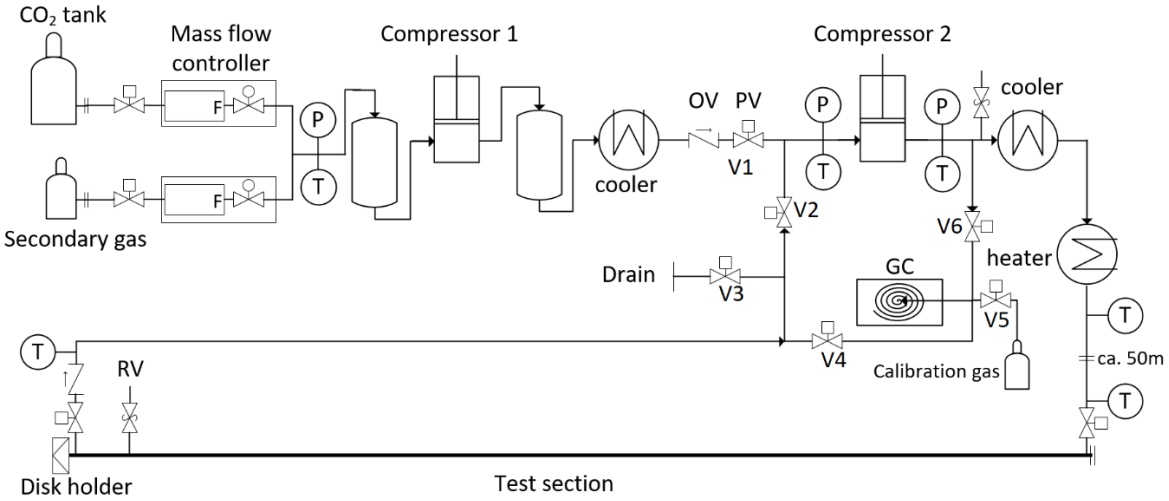

Figure 1: System overview of the ECCSEL depressurization facility (Munkejord et al., 2020). (RV: relief valve; OV: one-way valve; PV: pneumatic valve)

The experimental procedure is as follows. First, the rupture disk is installed and the system is evacuated. Then, the test section is filled with CO_2 and pressurized. When the pressure reaches approximately 70% of the desired pressure, the CO_2 is circulated to achieve a uniform temperature in the test section. The temperature is adjusted using the heating elements wrapped around the test section. The pressure is then increased gradually, with alternating filling and circulation of CO_2, until the disk ruptures. Upon disk rupture, the two pneumatic valves at the ends of the test section are automatically closed to stop circulation. The released CO_2 is vented through an exhaust pipe. An image of the CO_2 plume released from the exhaust pipe in Test 4 is shown in Figure 2.

Figure 2: Image of CO_2 plume released from the exhaust pipe in depressurization test 4.

2.2. Instrumentation

In the experiments studied, two kinds of rupture discs have been applied. Both of which have a specified burst pressure of 120 barg±5% at 22 °C. We study tests 4, 6, 8 and 19 of the ECCSEL depressurization facility. For tests 4, 6 and 8, X-scored discs were used, whereas for Test 19, a circular-scored triple-layer disc was employed. The initial conditions of the tests are presented in Section 4, Table 1. Along the test section of the facility, 16 fast-response pressure transducers and 23 thermocouples are mounted to the inner-surface in order to capture the pressure and temperature transients during depressurization. Most of the pressure sensors are densely distributed close to the open end to capture the expansion wave, as shown in Figure 3.

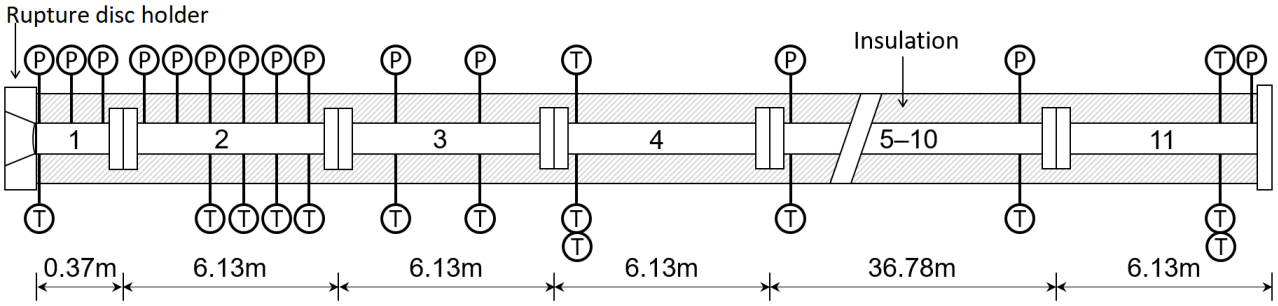

Figure 3: Test section of the ECCSEL depressurization facility (Munkejord et al., 2020). (Dimensions are not to scale, pipes 5-10 and corresponding sensors are omitted)

For our analysis, we will only use data from the first pressure transducer as it is closest to the pipe outlet and therefore experiences the most violent fall in pressure and records a large degree of superheat. This pressure transducer is located at 0.080 m from the rupture disc. The logging frequency of the data from the pressure transducers is 100 kHz for the time frame considered. The uncertainty of the data is 60 kPa with a 95% confidence level. The reported initial conditions of the experiments were estimated from the data between 1 ms and 0.5 ms before disk rupture.

3. THEORY AND MODELLING

3.1. Flow at equilibrium – the homogeneous equilibrium model

In order to analyze the experimental results, 1D CFD simulations of equilibrium flow are provided as a reference. We then apply the homogeneous equilibrium model (HEM) as described by Munkejord and Hammer (2015), with the method of Hammer et al. (2013). HEM is based on two main assumptions for two-phase flow of liquid (l) and gas (g):

1. The flow is well-mixed (homogeneous) such that the two phases are transported at the same velocity, $u_l = u_g = u$, and
2. the liquid and gas are in mechanical, chemical and thermal equilibrium.

For full-bore depressurization, the assumption of homogeneous flow has been found to be fairly accurate (Brown et al., 2013).

The model equations are discretized using the FORCE scheme in space (Toro and Billett, 2000) and forward Euler in time, with a Courant-Friedrichs-Lewy (CFL) number of 0.9. The simulation is conducted over a 12m domain with 800 grid cells. For the calculation of thermodynamic properties, the equation of state (EOS) of Span and Wagner (1996) is applied.

3.2. Nucleation theory and the superheat limit

Energy is required for bubbles to form in a metastable liquid. Boiling due to depressurization is interesting because nearly no energy is added from the outside environment, and large degrees of superheat can be reached before enough energy is available for bubble formation. This can be described by nucleation theory.

During nucleation, random thermal fluctuations cause the formation of small embryos of a new phase within the metastable phase. A certain free-energy barrier must be surpassed by the thermal fluctuations in order to create critically-sized embryos of the new phase. These embryos are just large enough to avoid collapsing back to the mother phase. As this is an activated process, the nucleation rate of critically-sized embryos can be expressed as an Arrhenius-type law,

$$J = K\, exp\left(-\frac{\Delta G^*}{k_B T}\right), \qquad \text{Eq. (1)}$$

where ΔG^* is the free-energy barrier, k_B is the Boltzmann constant, T is the temperature of the mother phase and K is a kinetic prefactor.

There are two main modes of nucleation, homogeneous and heterogeneous. Homogeneous nucleation occurs in the bulk of the liquid and the nucleation rate can be estimated with classical nucleation theory (CNT). Heterogeneous nucleation occurs on some surface or impurity, which lowers the free-energy barrier. The rate of heterogeneous nucleation can be estimated by multiplying the free-energy barrier found in CNT by some reduction factor (Debenedetti, 1996). However, no successful, rigorous model of this reduction factor currently exists for practical purposes, and correlations are often applied.

The following description of CNT is adapted from Debenedetti (1996). The free-energy barrier in CNT is estimated to be

$$\Delta G^* = \frac{4\pi\sigma r^{*2}}{3}, \qquad \text{Eq. (2)}$$

where σ is the surface tension and r^* the critical radius of the embryo. It is assumed that the surface tension of the embryo is equal to the planar surface tension between the phases at equilibrium. For bubble formation in a metastable liquid, the critical radius is approximated as

$$r^* = \frac{2\sigma}{p_{sat}(T_l) - p_l}, \qquad \text{Eq. (3)}$$

where $p_{sat}(T_l)$ is the saturation pressure at the liquid temperature and p_l is the liquid pressure. The kinetic prefactor can be approximated by

$$K = \widetilde{\rho_l}\sqrt{\frac{2\sigma}{\pi m}}, \qquad \text{Eq. (4)}$$

where $\widetilde{\rho_l}$ is the number density of liquid particles and m is the mass of one molecule. For completeness, we also provide the critical radius and kinetic prefactor for the formation of droplets in a metastable gas:

$$r^* = \frac{2\sigma}{\widetilde{\rho_l} k_B T\, ln(p_g/p_{sat})}, \qquad \text{Eq. (5)}$$

$$K = \frac{\widetilde{\rho_g}^2}{\widetilde{\rho_l}}\sqrt{\frac{2\sigma}{\pi m}}, \qquad \text{Eq. (6)}$$

$\widetilde{\rho_g}$ is the number density of gas particles.

In order to estimate the superheat limit (SHL), a critical nucleation rate is set to define the point where sudden phase change is observed. Following Aursand et al. (2017), we choose the critical nucleation rate to be $J_{crit} = 10^{12}\mathrm{m}^{-3}\mathrm{s}^{-1}$. The SHL is then found by solving for the temperature where

$$J(T) = J_{crit}. \qquad \text{Eq. (7)}$$

To determine the SHL, the properties of pure CO_2 in the stable and metastable regions is calculated using the Span and Wagner (1996) EOS and the CO_2 surface tension is approximated using the correlation of Rathjen and Straub (1977).

4. RESULTS AND DISCUSSION

In this section, the depressurization data of selected experiments from Munkejord (2020) and a new experiment from the ECCSEL depressurization facility are analyzed to find the degree of superheat reached. The result is compared to the superheat limit (SHL) predicted by CNT.

4.1. Experimental results

The conditions of the experiments are presented in Table 1. All the experiments were full-bore, meaning that no restriction was present at the outlet. For Test 19, two initial conditions are provided as the layers of the triple-layer rupture disk did not break at the same time, so a different condition was reached before the disk was fully opened. We estimate the temperature before the final layer of the rupture disk broke by assuming that the depressurizations due to other layers breaking were isentropic.

Table 1: Experimental conditions of the depressurization tests. Test 19 has two values provided; initial condition before first layer of rupture disk broke/initial condition before final layer of rupture disk broke.

Test no.	Pressure avg. (MPa)	Temperature avg. (°C)	Ambient temp. (°C)
4*	12.54	21.1	22
6*	10.40	40.0	6
8*	12.22	24.6	9
19	12.47/11.20	10.2/9.0	18

* Munkejord et al. (2020)

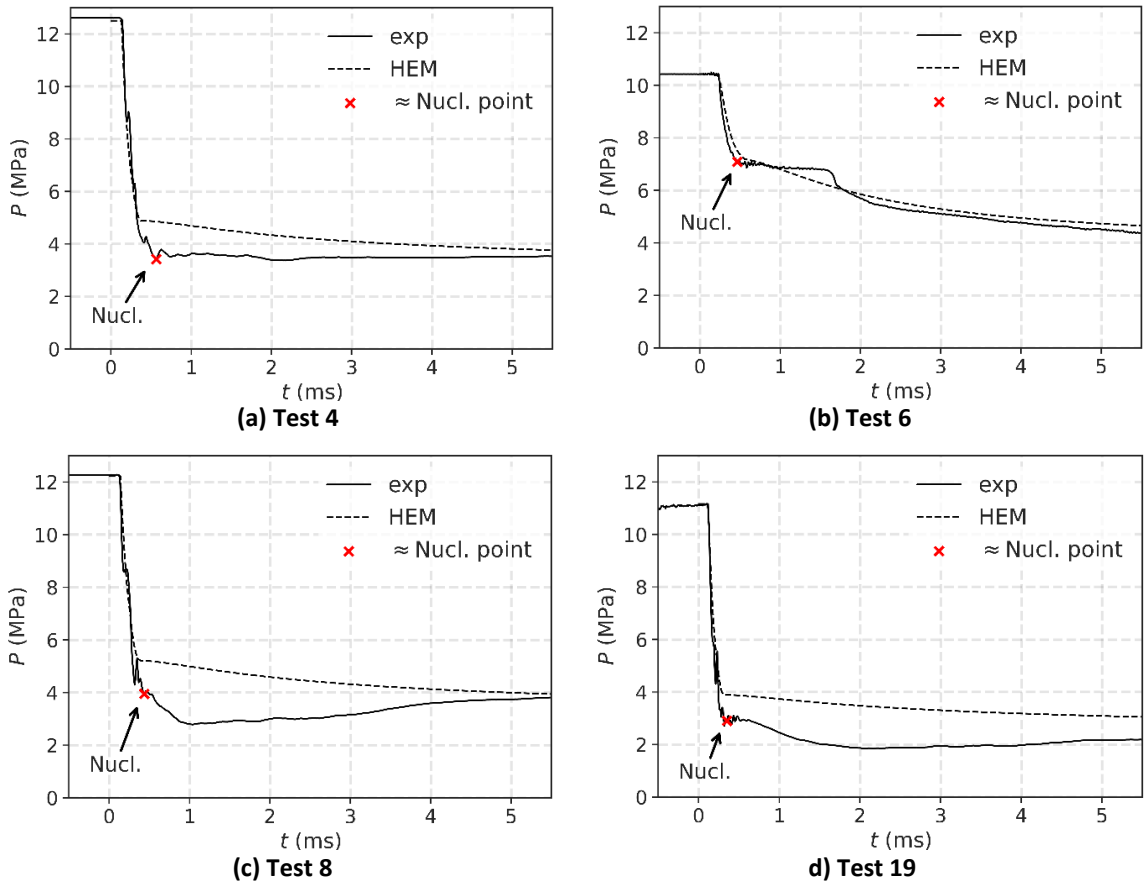

Figure 4: Data from the first pressure transducer over time (exp) for the tests presented in Table 1 compared to the HEM. Arrows and red crosses indicate approximately when bubble nucleation occurred in the experiments.

In Figure 4, the pressure measurements at 0.080 m from the open end is shown for all the tests from 0.5 ms before the rupture disk breaks until 5.5 ms has passed. The results are compared to HEM simulations.

The pressure falls very quickly when the CO_2 is in the liquid phase. As bubbles nucleate, the slope of the pressure time gradient reduces significantly and pressure perturbations can be observed. Based on this, we have marked with arrows the approximate area where nucleation occurred in the experiments. For tests 4, 8 and 19, nucleation of gas occurs at a lower pressure than what is predicted by HEM. For Test 6, nucleation occurs close to the point predicted by HEM, as this is very close to the critical point of CO_2. This is in line with nucleation theory.

4.2. Analysis and comparison to CNT

For further analysis, we choose a particular point for each test, marked with red crosses in Figure 4, to represent the point of nucleation. The exact choice of this point is somewhat uncertain, but it is based on the sudden flattening in the slope of pressure changes over time in combination with pressure perturbations. For such a short timeframe, it is reasonable to assume that the depressurization follows the liquid isentrope until nucleation occurs. We may then estimate the temperature at the point of nucleation. The information on the approximate point of nucleation is summarized in Table 2.

Table 2: Summary on the approximate point where nucleation starts for the ECCSEL depressurization tests and comparison to the homogeneous SHL predicted by CNT.

Test no.	Time (ms)	P (MPa)	T (K)	Exp. superheat (K)	Hom. SHL (K)	Rel. diff. (%)
4	0.56	3.43	283.9	11.3	11.1	2%
6	0.47	7.17	302.9	0.0	0.0	0%
8	0.44	3.95	287.1	9.1	8.2	11%
19	0.32	2.70	274.1	10.3	16.7	-38%

Finally, we plot the approximate points where nucleation first occurred for the ECCSEL depressurization tests in a temperature-pressure diagram and compare this to the homogeneous SHL predicted by CNT. The result is shown in

Figure 5.

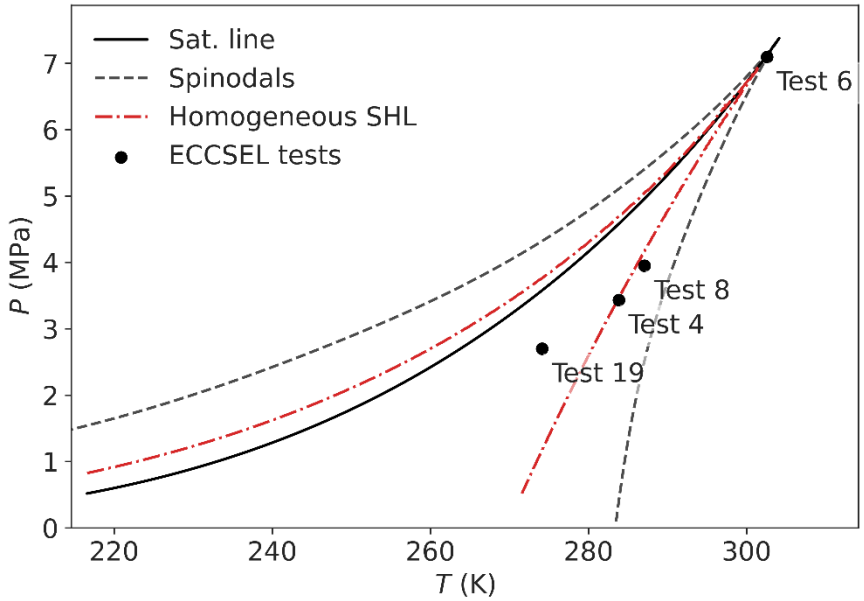

Figure 5: Approximate (p,T)-points of nucleation for the ECCSEL depressurization tests, assuming an isentropic depressurization path. Tests 4, 6, and 8 agree well with the homogeneous SHL predicted by CNT.

The nucleation points of tests 4, 6 and 8 agree very well with the superheat limit predicted by CNT. For Test 19, the superheat reached experimentally is 7.2 K lower than that predicted by CNT. This is likely caused by

heterogeneous nucleation at the wall of the test section. At lower temperatures it is expected that heterogeneous nucleation will dominate over homogeneous nucleation, so the result is reasonable.

The results indicate that the degree of superheat can be predicted quite accurately by the superheat limit derived from CNT for higher temperatures. In turn this can be used to predict mass flow rates in process equipment. At temperatures below about 280 K, heterogeneous nucleation begins to dominate, and more data will be needed in order to create a predictive model or correlation to predict the limit of superheat. However, the available data for this analysis are quite scarce. It would be interesting to see how the effect of heterogeneous nucleation changes both at lower temperatures and with different degrees of wall-roughness in the test section. This could be a fruitful avenue of further research.

5. CONCLUSIONS

In many industrial applications, it is relevant to predict the degree of superheat reached by liquid CO_2 before phase change is initiated during expansion. In the present work, the pressure data of pure CO_2 depressurization tests at the ECCSEL facility has been analyzed and the degree of superheat reached has been determined. The degree of superheat agrees well with the homogeneous superheat limit predicted by CNT for high temperatures, near the critical point. At lower temperatures, a lower degree of superheat is reached in the experiments due to heterogeneous nucleation.

ACKNOWLEDGEMENTS

This paper has been produced with support from the NCCS Centre, performed under the Norwegian research programme Centres for Environment-friendly Energy Research (FME) and the Research Council of Norway (257579).

The construction of the ECCSEL Depressurization Facility was supported by the INFRASTRUKTUR programme of the Research Council of Norway (225868).

NOMENCLATURE

Latin letters

R_a	Mean roughness of pipe (m)	J	Nucleation rate (critical-size embryos $m^{-3}s^{-1}$)
u	Velocity in x-direction (ms^{-1})	K	Kinetic prefactor (embryos $m^{-3}s^{-1}$)
k_B	Boltzmann constant ($1.380649\times 10^{-23} m^2kgs^{-2}K^{-1}$)	T	Temperature (K)
ΔG^*	Free-energy barrier of formation for critical-size embryo (J)	r^*	Radius of critical-size embryo (m)
p	Pressure (Pa)	m	Molecular mass (kg)

Greek letters

$\widetilde{\rho}$	Number density (molecules m^{-3})	σ	Surface tension (Nm^{-1})

Subscripts

l	Liquid phase	g	Gas phase
sat	At saturation	$crit$	At critical nucleation point/ superheat limit

Abbreviations

CCS	CO_2 capture and storage	CFD	Computational fluid dynamics
HEM	Homogeneous equilibrium model	EOS	Equation of state
CNT	Classical nucleation theory	SHL	Superheat limit

REFERENCES

Aursand, P., Gjennestad, M., Aursand, E., Hammer, M., Wilhelmsen, Ø., 2017. The spinodal of single- and multi-component fluids and its role in the development of modern equations of state. Fluid Phase Equilib. 436, 98-112.

Brown, S., Martynov, S., Mahgerefteh, H., Proust, C., 2013. A homogeneous relaxation flow model for the full bore rupture of dense phase CO2 pipelines. Int. J. Greenh. Gas Control. 17, 349-356.

Debenedetti, P.G, 1996. Metastable Liquids: Concepts and Principles. Princeton University Press, Princeton, 412.

ECCSEL, Depressurization facility, http:// eccsel2020.promoscience.com/facilities /transport/no25_sintef_er_depress, Accessed 24 Jan 2022.

Hammer, M., Ervik, Å., Munkejord, S.T., 2013. Method Using a Density-Energy State Function with a Reference Equation of State for Fluid-Dynamics Simulation of Vapor-Liquid-Solid Carbon Dioxide. Ind. Eng. Chem. Res. 52(29), 9965-9978.

Munkejord, S.T., Hammer, M., 2015. Depressurization of CO2-rich mixtures in pipes: Two-phase flow modelling and comparison with experiments. Int. J. Greenh. Gas Control. 37, 398-411.

Munkejord, S.T., Austegard, A., Deng, H., Hammer, M., 2020. Depressurization of CO2 in a pipe: High-resolution pressure and temperature data and comparison with model predictions. Energy. 211, 118560.

Rathjen, W., Straub, J., 1977. Surface tension and refractive index of six refrigerants from triple point up to critical point, 7th Symposium on Thermophysical Properties, American Society of Mechanical Engineers, 839-850.

Span, R., Wagner, W., 1996. A new Equation of State for Carbon Dioxide Covering the Fluid Region from the Triple-Point Temperature to 1100 K at Pressures up to 800 MPa. J. Phys. Chem. Ref. Data. 25(6), 1509-1596.

Toro, E.F., Billett, S.J., 2000. Centred TVD schemes for hyperbolic conservation laws. IMA J. Numer. Anal. 20(1), 47-79.